AIAA JOURNAL
Vol. 49, No. 5, May 2011

# Proper Orthogonal Decomposition Analysis of Coherent Structures in Simulated Reacting Buoyant Jets

X. Zhou* and D. L. Hitt†
*University of Vermont, Burlington, Vermont 05405*

DOI: 10.2514/1.J050475

**The spatial evolution of a circular reacting buoyant jet at moderate Reynolds number ($Re = 10^3$) has been investigated using large-eddy simulation. Infinitely fast chemistry of a Burke–Schumann formulation is employed to model the combustion process in a reacting buoyant jet. Dynamic puffing phenomena is observed and corresponds to the formation of large-scale vortex structures near the plume base. These toroidal vortical structures break down into smaller, disorganized eddies with increasing distance downstream. Two-point correlation variances of temperature and velocities generated from large-eddy simulation are analyzed using the proper orthogonal decomposition method. The energy of the flow is found to be well represented by a finite number of eigenmodes. Further, the corresponding eigenfunctions accurately capture the large-scale coherent structures: namely, the vortex rings in the laminar region and a large-scale strong helical motion in the turbulent region. In the near-field region the dominant vortex-shedding frequency obtained from Fourier analysis agrees well with experimental data. Proper orthogonal decomposition analysis in the transitional and turbulent regions reveals the dominance of subharmonic frequencies, indicating vortex merging in the downstream flow that cannot be detected from Fourier analysis of raw large-eddy simulation data.**

## I. Introduction

BUOYANT jets and plumes are of practical interest in the study of many engineering, industrial, and environmental flows. One important effect of buoyancy in a jet is to enhance the entrainment of the surrounding fluid in comparison to nonbuoyant jets [1,2]. Buoyant flows are characterized by two-dimensional, organized, large vortex structures, and a self-sustained puffing phenomenon close to the plume base. In most buoyancy-dominated flows the pulsation frequency has been experimentally observed to be insensitive to the Reynolds number and coflow (surrounding the primary flow) velocity, but strongly dependent on the Froude number [3], density ratio of the injected to ambient fluid [4] and thermodynamic pressure [5]. Mell et al. [6] showed that the shedding frequencies for both diffusion flames and nonreacting plumes overlapped over a wide range of conditions, suggesting that the controlling mechanism might be similar. Specifically, in combusting flows the pulsation frequency is rather insensitive to the heat release rate, the type of fuel, and the stoichiometric ratio [6,7]. The buoyancy-induced instability has been discussed from a theoretical point of view [8,9] and confirmed by numerical investigations to be directly related to the formation and evolution of large-scale vortex structures [10]. Similar to the nonreacting case, a reacting plume undergoes transition from laminar to turbulent flow with a subsequent breakdown in the near field. The near-field vortex dynamics are also expected to be crucial for the control of instability and the transitions from laminar to turbulent and from jetlike to plumelike behavior in a buoyant jet flame.

Self-similar behavior in jet flames, independent of initial conditions in the far field, has been well studied by using Reynolds-averaged numerical simulation (RANS) combined with the conditional moment closure (CMC) [11], probability density function (PDF) [12] and flamelet methods [13] in practical applications. However, the flame-vortex interactions in the transitional region, which is of particular interest, can only be examined either by direct numerical simulations (DNS) or large-eddy simulation (LES). Some direct numerical simulations have been conducted of the buoyancy effect on dynamic behavior of plumes and flames [6,14,15]. Jiang and Luo [14,15] investigated nonreacting and reacting plumes using DNS. Good agreement has been achieved for the pulsation frequencies between their numerical results and available experimental data. Their studies have also included detailed examination of the geometry and side-wall effects. Large-eddy simulation (LES) is more attractive than DNS in the flows of higher Reynolds number and complex geometries in the sense that it needs much less computer resources and CPU time. LES has proven to be an effective tool in simulating transitional flows as well (e.g., [16]). For plumes in particular, with LES it is possible to capture the laminar near-field puffing behavior, the transition to turbulence, and the self-similar, fully turbulent behavior further downstream [10,17].

Proper orthogonal decomposition (POD) [18] is a powerful low-dimensional analysis tool that can be used to examine coherent structures embedded in turbulent flows. It has drawn significant interest for its use in constructing reduced-order models of complex flows. For example, it has been applied in flows such as mixing layers [19], high-speed jets [20], turbulent wake flows [21], channel flows [22], planar jets [23], and buoyant jet [24]. LES can provide a large amount of information of small- and large-scale eddies of the turbulent flow at relatively high Reynolds numbers. By using the POD method, the most energetic coherent structures can be extracted by decomposing the fluctuating field obtained from LES into a linear sum of orthogonal eigenfunctions representing temporal or spatial correlations. The advantage of representing the largest scales of motion is also of great interest to reacting buoyant jets.

The objective of this work is to examine and compare large-scale coherent structures in buoyant reacting jets, and builds upon the previous study by Zhou and Hitt [24], which entailed 2-D POD analyses of heated, buoyant (nonreacting) jets at moderate Reynolds numbers ($Re \sim 1000$). These flow are simulated using LES and analyzed using the POD method. We adopt a one-step, irreversible, and infinitely fast chemical reaction as a model for the combustion process. First, the implemented LES techniques and POD method are discussed briefly. Next, we examine the large-scale coherent structures by conducting a two-dimensional POD analysis of the temporal two-point correlations of velocity and temperature fields.

Presented as Paper 2005-5147 at the 35th AIAA Fluid Dynamics Conference and Exhibit, Toronto, Ontario, Canada, 6–9 June 2005; received 3 February 2010; revision received 6 August 2010; accepted for publication 7 December 2010. 

*Research Assistant Professor, Mechanical Engineering Program, School of Engineering.

†Associate Professor, Mechanical Engineering Program, School of Engineering. Associate Fellow AIAA.

From this, The most energetic coherent structures are obtained and represent the dominant modes present in reacting buoyant jet. The validity of a 2-D POD analysis can justified in the present study, as in [24], given the focus is restricted to the near-field region of the jet consisting of laminar and transitional flow; supporting evidence for this assumption also exists in the experimental literature (e.g., Glauser and George [25]).

## II. Computational Methods

### A. Governing Equations

A global one-step irreversible chemical reaction is adopted: $F + sO \rightarrow (1+s)P$, where $s$ is the stoichiometric ratio and $F, O, P$ denotes the fuel, oxidant, and product, respectively. The infinitely fast-chemistry of the Burke–Schumann formulation is assumed and, therefore, the instantaneous mass fractions of fuel, oxidant, and product can be directly related to the instantaneous mixture fraction $Z$. The temperature can be obtained through the relationship of enthalpy and mass fraction of fuel, $h = c_p T + m_{fu}\Delta H_{fu}$, where $\Delta H_{fu}$ is the heat release rate.

The large-eddy simulation methodology is employed to simulate the three-dimensional time-dependent jet flow. For a low Mach number, variable density flow, the governing (filtered) equations for continuity, momentum, energy, and mixture fraction are given by [17]

$$\frac{\partial \bar{\rho}}{\partial t} + \frac{\partial}{\partial x_j}(\bar{\rho}\tilde{u}_j) = 0 \tag{1}$$

$$\frac{\partial(\bar{\rho}\tilde{u}_i)}{\partial t} + \frac{\partial(\bar{\rho}\tilde{u}_i\tilde{u}_j)}{\partial x_j} = -\frac{\partial \bar{p}^{(1)}}{\partial x_i} + \frac{\partial \bar{\sigma}_{ij}}{\partial x_j} + (\rho_a - \bar{\rho})g_i - \frac{\partial \tau_{ij}}{\partial x_j} \quad (i = 1,2,3) \tag{2}$$

$$\frac{\partial(\bar{\rho}\tilde{h})}{\partial t} + \frac{\partial(\bar{\rho}\tilde{u}_j\tilde{h})}{\partial x_j} = \frac{\partial}{\partial x_j}\left[\left(\frac{\lambda}{C_p}\right)\cdot\frac{\partial \tilde{h}}{\partial x_j}\right] - \frac{\partial Q_j}{\partial x_j} \tag{3}$$

$$\frac{\partial(\bar{\rho}\tilde{Z})}{\partial t} + \frac{\partial(\bar{\rho}\tilde{u}_j\tilde{Z})}{\partial x_j} = \frac{\partial}{\partial x_j}\left[(\bar{\rho}\mathcal{D})\cdot\frac{\partial \tilde{Z}}{\partial x_j}\right] - \frac{\partial M_j}{\partial x_j} \tag{4}$$

where $\tilde{u}_i = \overline{\rho u}_i/\bar{\rho}$ and $\tilde{h} = \overline{\rho h}/\bar{\rho}$, $\tilde{Z} = \overline{\rho Z}/\bar{\rho}$ are the Favre-filtered velocity enthalpy and mixture fraction. Ideal gas behavior is assumed so that the mean density $\bar{\rho}$ can be obtained from $p^{(0)} = \bar{\rho}RT$, with the zeroth-order thermodynamic pressure $p^{(0)}$ equal to the atmospheric pressure. Summation over the three coordinate directions is implied in terms of repeated indices. The quantities $\rho_a$, $\bar{p}^{(1)}$, $\lambda$, and $C_p$ are the density of ambient air, pressure, thermal conductivity, and specific heat. The molecular viscosity, thermal conductivity, and specific heat are denoted by $\mu$, $\lambda$, and $C_p$, respectively. The nonresolvable small-scale turbulence can be represented by a subgrid scale (SGS) model (e.g., Smagorinsky, similarity, gradient, and dynamic models). In particular, the widely used, standard Smagorinsky SGS model (constant coefficient) has proven capable of producing accurate results for buoyant jet flows [10,17]. The SGS Reynolds stress $\tau_{ij}$ follows the form of the molecular viscous stress $\bar{\sigma}_{ij}$ but with a negative sign and both stresses are given by

$$\tau_{ij} = \overline{\rho u_i u_j} - \bar{\rho}\tilde{u}_i\tilde{u}_j \equiv -\mu_e\tilde{S}_{ij}\bar{\sigma}_{ij} = \mu\tilde{S}_{ij} \tag{5}$$

where $\mu$ is the molecular viscosity

$$\tilde{S}_{ij} = \left(\frac{\partial \tilde{u}_i}{\partial x_j} + \frac{\partial \tilde{u}_j}{\partial x_i}\right) - \frac{2}{3}\frac{\partial \tilde{u}_k}{\partial x_k}\delta_{ij} \tag{6}$$

is the rate-of-strain tensor and

$$\mu_e = \bar{\rho}C_s^2\Delta^2\sqrt{\frac{1}{2}\tilde{S}_{ij}\tilde{S}_{ij}} \tag{7}$$

is the eddy viscosity. Note that $\Delta = (\Delta x \Delta y \Delta z)^{1/3}$ is a characteristic length based on the local grid resolution and $C_s(=0.1)$ is a constant. The subgrid scale heat flux $Q_j$ is defined according to

$$Q_j = \overline{\rho u_j h} - \bar{\rho}\tilde{u}_j\tilde{h} = -\frac{\mu_e}{Pr_e}\frac{\partial \tilde{h}}{\partial x_j}, \qquad M_j = \overline{\rho u_j Z} - \bar{\rho}\tilde{u}_j\tilde{Z} = -\frac{\mu_e}{Sc_e}\frac{\partial \tilde{Z}}{\partial x_j} \tag{8}$$

where $Pr_e$, $Sc_e$ is the eddy Prandtl number and Schmidt number (=0.3 here). The gravitational term $g_i$ represents the buoyancy force.

The details of the numerical implementation can be found in [10,17], but are summarized here for completeness. A second-order central-difference scheme is used for the spatial discretization and an Adams–Bashforth scheme is used for the temporal integration. A staggered uniform Cartesian grid is employed in which the scalar variables are stored at the cell centers while the velocity components are specified at the cell faces. The time step is chosen such that the maximum Courant–Friedrichs–Lewy (CFL) number is less than 0.3 for stability. The projection method, which is composed of prediction and correction steps, is used for the velocity field. The Poisson equation coupling the momentum and continuity equations is solved by a multigrid method. The imposed boundary conditions include inflow, outflow, and lateral entrainment boundaries. At the inflow, the velocities $u_i$ and temperature are specified. A uniform inflow temperature is assumed. To excite the flow, uniformly distributed random perturbations are superimposed on an inflow velocity profile of the following "top-hat" form:

$$U(r) = \frac{1}{2}U_0\left[1 - \tanh\left[b_2\left(\frac{2r}{D} - \frac{D}{2r}\right)\right]\right] \tag{9}$$

Here $U_0$ is the inflow mean axial velocity and $b_2$ is a parameter that strongly influences the shear-layer instability; in this work we have chosen $b_2 = 20$ [24]. Low-amplitude (1%) random perturbations with zero mean values are applied to the inlet velocity at each time step. At the lateral domain boundaries a constant pressure condition is imposed, thus ambient fluid can be entrained into the plume through the surface. A zero velocity gradient (or outflow) boundary condition is applied at the outlet and the axial velocity is constrained to be positive to ensure numerical stability.

A proper orthogonal decomposition can be performed on the jet data generated by the LES to analyze the intrinsic large-scale coherent structures. The underlying principle of POD is that it yields a set of numerical eigenfunctions that are optimal in energy and which have the largest projection. This approach has been successfully used in a previous study by the authors that examined coherent structures in transient heated jets [24]. In the following section, we show that the spatio-temporal behavior of the buoyant jet can be well represented using a finite number of eigenfunction modes.

### B. POD Method

A proper orthogonal decomposition can be performed on the jet data generated by the LES to analyze the intrinsic large-scale coherent structures. The underlying principle of POD is that it yields a set of numerical eigenfunctions that are optimal in energy and which have the largest projection. In this work, the snapshot method of Sirovich [26] and Ma and Karniadakis [27] is used to solve the associated eigenvalue problem.

The POD implementation is as follows. We assume there exists an ensemble of $M$ discrete instantaneous flow variables $\psi(\mathbf{x}, t_k)$ (fluctuating velocity or temperature here) acquired at times $t_k$ $(k = 1, 2, \ldots M)$ on a two-dimensional domain $A$. POD analyses are performed primarily on two-dimensional slices along the streamwise direction ($x$-$y$ plane) and to a lesser degree in transverse ($y$-$z$) planes at various streamwise locations. The full grid resolution of the LES data is used. We can construct the two-point temporal correlation matrix $C$ containing the following elements

$$C(t_j, t_k) = \frac{1}{M}\int_A \psi(\mathbf{x}, t_j)\psi(\mathbf{x}, t_k)\,\mathrm{d}\mathbf{x}, \qquad (j, k = 1, 2, \ldots M) \tag{10}$$

The set of $M$ eigenvalues $\lambda$ and eigenmatrix $\mathbf{a}$ corresponding to the correlation matrix $C$ are obtained as solutions to the equation

$$\mathbf{Ca} = \lambda\mathbf{a} \tag{11}$$

Equation (11) can be solved numerically using the MATLAB® software package in this work. The POD eigenfunctions $\phi^n$ at a mode $n$ can then be written as linear combinations of the instantaneous fluctuating flowfield:

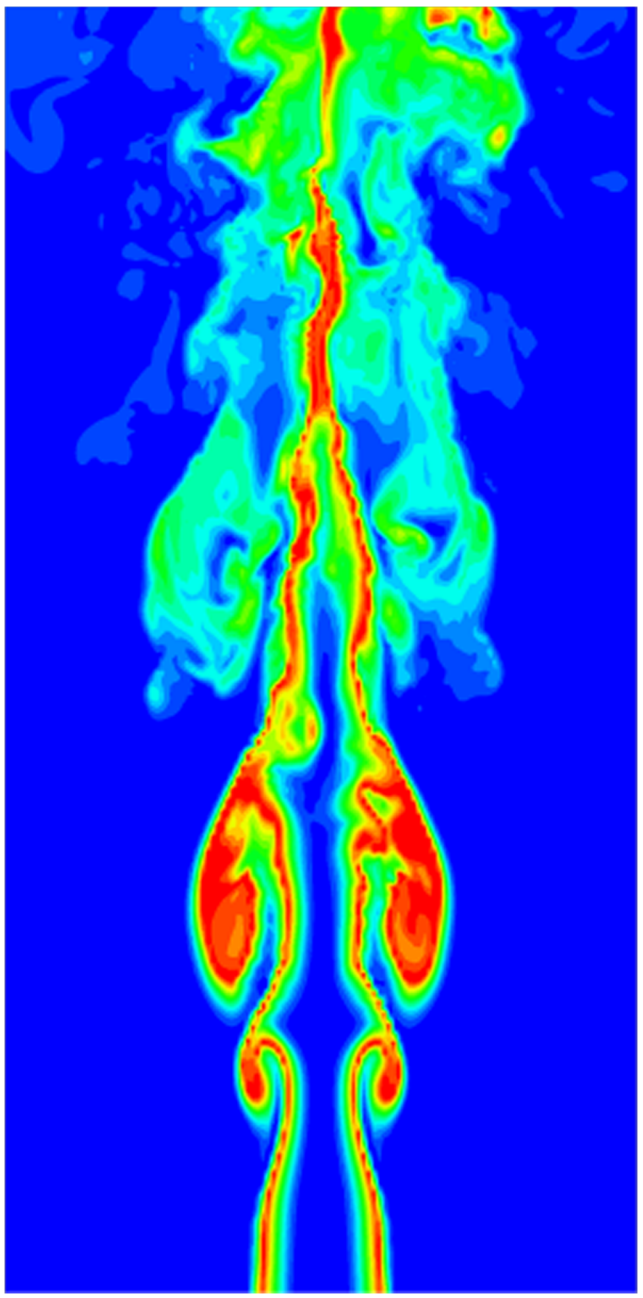

**Fig. 1 Flow visualization of instantaneous temperature contours on a midplane of a reacting jet as simulated by LES. The Reynolds number is 1000 based on the base inlet conditions. The plume domain is 12 × 6 × 6 inlet diameters in size with corresponding grid resolution 256 × 128× 128 cells.**

$$\phi^n(\mathbf{x}) = \sum_{k=1}^{M} a_k^n \psi(\mathbf{x}, t_k) \tag{12}$$

The POD modes are mutually orthogonal according to:

$$\sum_{i=1}^{N_1}\sum_{j=1}^{N_2} \phi^m(x_{i,j})\phi^n(x_{i,j}) = \delta_{mn} M\lambda^n \tag{13}$$

$$\sum_{k=1}^{M} a_k^m a_k^n = \delta_{mn} \tag{14}$$

Here, $\delta_{mn}$ is the Kronecker delta and $N_1$, $N_2$ are the number of grid points along each of the coordinate directions of the plane slice.

One may then reconstruct the instantaneous flowfield using the numerical eigenfunctions:

$$\tilde{\psi}(\mathbf{x}, t_k) = \sum_{n=1}^{N_{\mathrm{POD}}} a_k^n \phi^n(\mathbf{x}) \tag{15}$$

where $N_{\mathrm{POD}}$ is the number of POD modes to be used for reconstruction. In the following section, we show that the spatio-temporal behavior of the buoyant reacting jet can be well represented using a finite number of eigenfunction modes.

## III. Results and Discussion

In this section, we discuss the computational results for an unconfined buoyant jet diffusion flame with the fuel $CH_4$ as the primary fluid surrounded by oxidizer $O_2$ as ambient fluid. Simulations are performed for a vertically oriented circular jet subject to normal gravity conditions. The heat release rate is assumed to be $\Delta H_{fu} = 2.42 \times 10^6$ (J/mol) and the stoichiometric mixture fraction is $Z_{\mathrm{st}} = 0.2$. The heat release rate is chosen with the consideration of reducing computational requirement of LES by decreasing the peak or adiabatic temperature. The Reynolds number is 1000, based on the inflow mean velocity $U_0 = 1.0$ m/s and diameter $D = 6.35$ cm. The Froude number is $Fr = U_0^2/gD = 1.61$. A rectangular $(x, y, z)$ computational domain is used which extends 12 diameters in the streamwise $x$ direction and 6 diameters in both the lateral $(y, z)$ directions. The corresponding grid resolution is $512 \times 128 \times 128$ cells. This grid resolution has been previously demonstrated to provide reliable results for buoyant jet flows [10,17,24]. A characteristic convective time scale is defined as $\tau_c = D/U_0$ (=0.0635 s here) and about $300\tau_c$ of sampling time is needed to acquire sufficient statistical samples. Sampling is performed after a quasi-steady flow is achieved. A time step of $5 \times 10^{-5}$ s is used to ensure

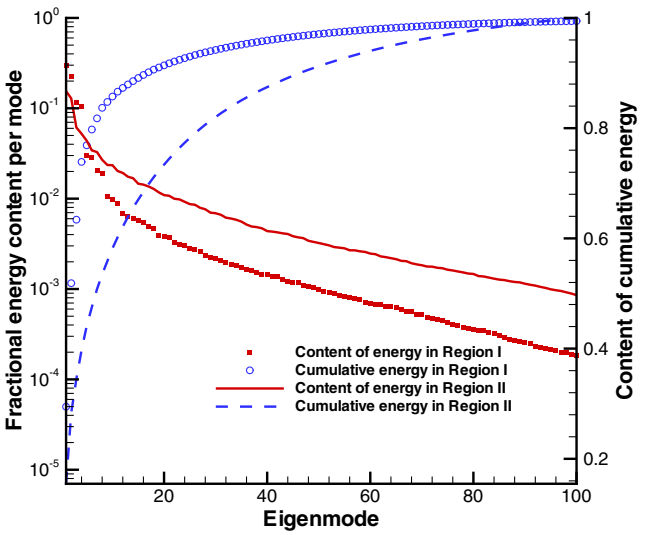


**Fig. 2 Fractional and cumulative energy contents at each POD mode. Shown in this plot are the separate cases of downstream Region I ($x$ = 0–6 diameters) and Region II ($x$ = 6–12 diameters).**

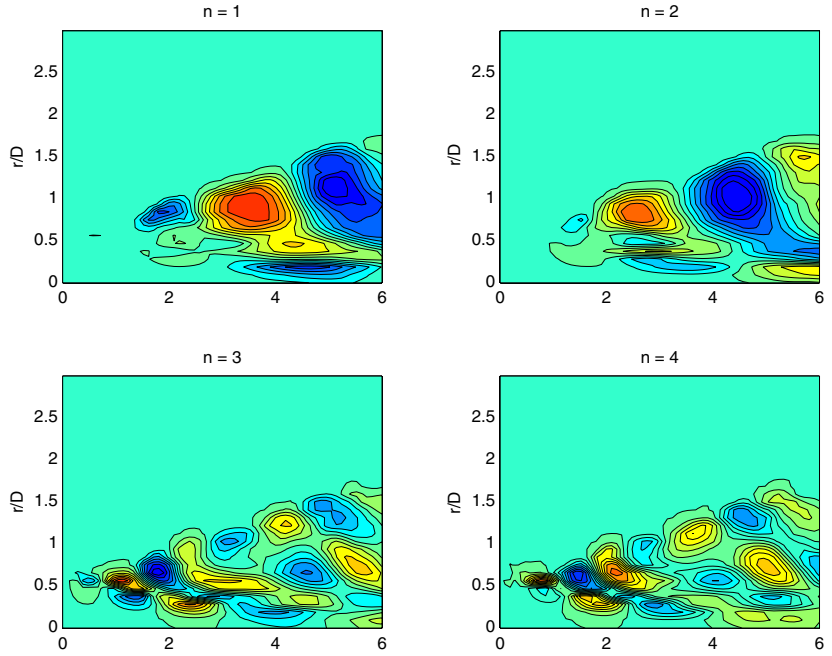


**Fig. 3 Contours of the fluctuating temperature eigenfunctions (normalized) for modes $n = 1 - 4$ on a midplane in Region I ($x = 0 - 6D$). Here $x$ is the streamwise distance and $r/D$ is the normalized radial position. An alternating modal structure is observed which corresponds to the vortical structures being shed.**

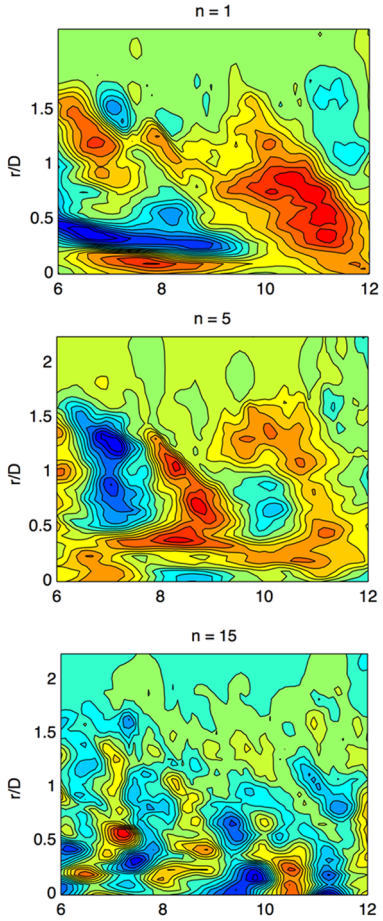


**Fig. 4 Contours of the fluctuating temperature eigenfunctions (normalized) for modes $n = 1$, 5, and 15 on a midplane in Region II ($x = 6 - 12D$). Here $x$ is the streamwise distance and $r/D$ is the normalized radial position.**

the CFL number is less than 0.3. Roughly 200 h are required for each simulation when running on two Linux-based computers (Dell PowerEdge 2650) with dual processors (2.8 GHz Xeon$^{TM}$) and 4 GB of RAM.

### A. Dynamic Puffing Behavior

A known characteristic of buoyant jets at this Reynolds number is a so-called "puffing" behavior. A sample snapshot of the instantaneous temperature contours at the $XY$ central-plane is shown in Fig. 1, where the large-scale vortex structures corresponding to the puffing phenomena are readily observed. From an animation of temperature snapshots, a highly repeatable pulsation behavior in the near field as well as the random motions in the far field can be observed. In the near field, which extends to about six diameters from the origin of the plume source, the buoyant reacting jet is characterized by organized, toroidal vortical structures. The onset of vortex shedding is understood to be primarily driven by buoyancy force due to the density inhomogeneity of the primary fluid $\rho_0$ from the ambient fluid $\rho_a$. It has been shown by Jiang and Luo [28] that the pulsation behavior cannot be produced without buoyancy effect in a jet diffusion flame by conducting a DNS. The rolled-up vortex sheets are filled with localized "pockets" of hot gaseous products of the chemical reaction near the stoichiometric mixture fraction $\tilde{Z} = Z_{st}$ where fuel and oxidizer are actively consumed. The continuous flame can be broken down into smaller eddies by high strain rates downstream of the flame. It can also be observed that the flame tip moves rather randomly due to the turbulent behavior as the secondary instability mode dominates the flow. The flame downstream appears to be nearly "pinching off" from the preceding flame tip, which is a result of the entrainment of cooler fluid toward the center region by the strong helical mode of instability. A certain regularity associated with coherent structures persists irrespective of the random motions and the transition to turbulence in the far field. These structures can be resolved by a POD analysis as shown in the following section.

### B. POD Analysis

A POD analysis has been performed using a total of 1500 sets of instantaneous flow "snapshots" sampled every 20 time steps (or about $0.063\tau_c$ apart). Here we examine two equally divided regions in the flow which are convenient for the POD analysis. There exists

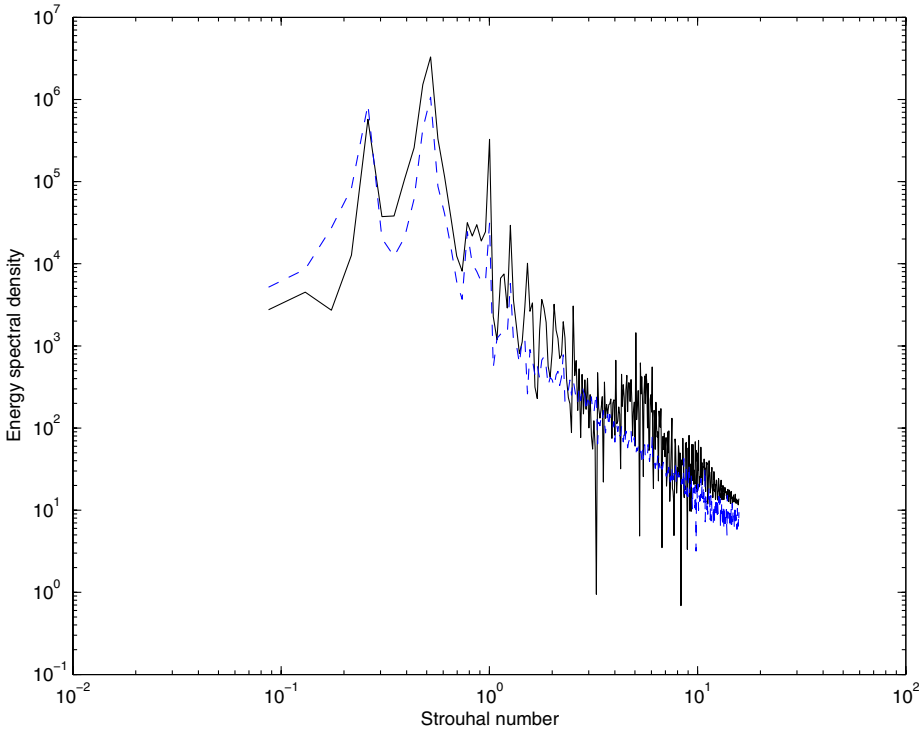


**Fig. 5 Power spectra of the fluctuating centerline velocities in the laminar region at $x/D = 3$. Shown is the spectrum of original LES data (solid line) and those obtained from POD reconstructions (dashed line). Note that only one mode is required to capture the fundamental frequency in the near-field region here.**

distinctive behavior in each of these two regions. The first region (I) is defined by $x \in \langle 0, 6D \rangle$ and remains essentially laminar. The second region (II) is defined by $x \in \langle 6D, 12D \rangle$ and features transitional and turbulent flow. By analyzing the eigenfunction modes of the temperature field in the two regions as shown in Fig. 2, it can be seen that in the near field (Region I) the first two modes contain nearly the same level of energy ($\sim$30%) and together account for a large portion of the total energy in the flow. The modal energy distribution decreases rapidly as the mode number increases and becomes negligible after a few modes. The data shows that 90% of the energy is contained in less than 10 modes, suggesting that this number of modes should be sufficient to capture the large-scale dynamics present in the near-field buoyant jet. In contrast, many more modes are necessary to capture the energy in the transitional jet region (Region II). Here the fundamental mode accounts for only $\sim$15% of the total energy and a much more gradual decrease in energy content

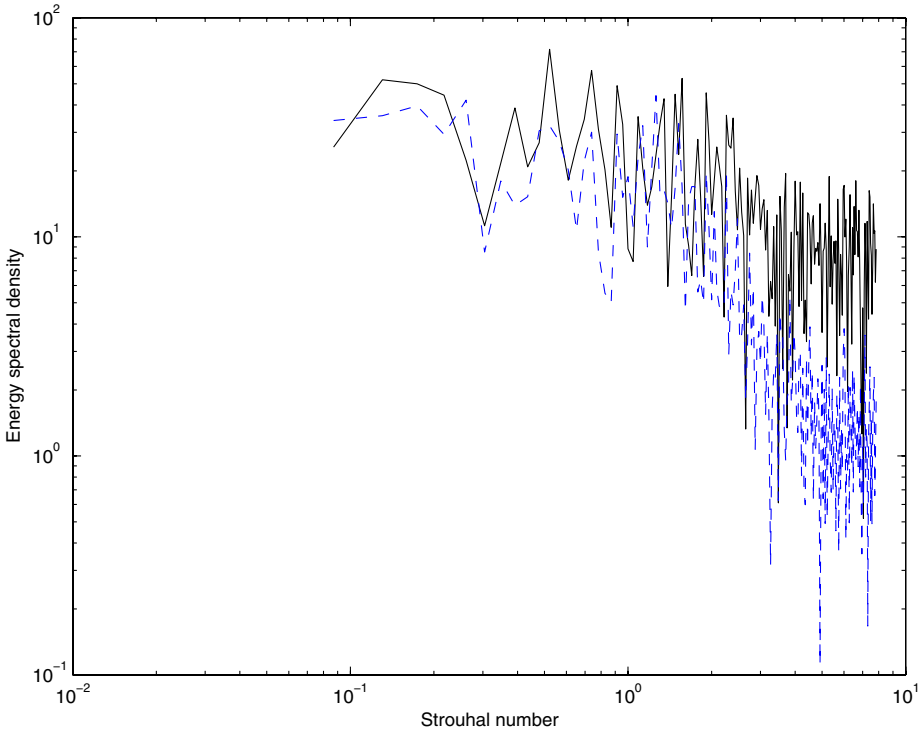


**Fig. 6 Power spectra of the fluctuating centerline velocities in the laminar region at $x/D = 9$. Shown is the spectrum of original LES data (solid line) and those obtained from POD reconstructions (dashed line). Approximately 12 modes are required to match the LES spectrum at this streamwise location. For the turbulent region, 20 modes are required to capture the LES specrtrum (refer to Fig. 7).**

is observed at higher modes. About 36 modes are required to capture 90% of the energy, whereas 20 modes can capture only about 70%. The differences in the energy distributions in Regions I and II are to be expected owing to the laminar and turbulent natures of the respective regions. In the laminar region, all of the energy is stored in large coherent structures which correspond to the first few eigenmodes. For the turbulent region there is the cascade of energy from large eddies to small length scales and the broader distribution of energy over various length scales is reflected in the modal distribution.

Figure 3 shows the first four eigenfunctions ($n = 1, 2, 3, 4$) of the temperature fluctuations obtained from a POD analysis in a $x$-$y$ midplane of Region I. Axisymmetric modes dominate in this region and therefore only the upper half domain is shown here. The odd and even modes occur naturally in "pairs." These pairs have similar eigenvalues and spatial structures of similar size. The spatial structures are phase-shifted in the streamwise direction. Coherent scales become smaller and smaller as the mode number of the eigenfunctions increases. Higher-mode eigenfunctions follow the same trends as the lower-order modes but contain less energy.

Figure 4 shows the eigenfunctions at the modes of 1, 5, 15, and 20 further downstream (Region II) in a midplane of the transitional and turbulent region. Although the instantaneous flowfield looks very random, the first eigenfunction still shows large-scale, organized structures. This is a direct result of the POD's ability to filter the fine-scale turbulent fluctuations from the random motions in the jet and resolve the large-scale coherent structures. In the higher modes ($n = 5$) several smaller coherent structures exist. For still higher modes ($n = 15, 20$) there is an increase of small-scale structures and more complex behavior.

### C. Fast Fourier Transform Amplitudes and Power Spectra

The power spectrum of the LES centerline radial velocity has been computed from a time series at the near-field location $x/D = 3, 9$ and appears in Figs. 5 and 6. The spectrum has been computed using conventional fast Fourier transform (FFT) techniques and without any additional signal processing or filtering methods applied.

Also shown in Fig. 5 are the corresponding spectra computed from POD-reconstructed velocities using the fundamental mode at $x/D = 3$. A dominant Strouhal number, $St = fD/U_0 = 0.51$, is observed with an equivalent frequency of $f = 8.5$ Hz. The first eigenmode is able to accurately capture the fundamental frequency as expected, since it is derived from the large-scale coherent structures in the flow. However, it shows a little lower spectra amplitudes and it fails to capture the higher harmonics corresponding to smaller structures. It is clear that even though random disturbances have been imposed at the inflow plane, the buoyant jet still shows a highly regular, puffing behavior in the near-field region as would be observed in purely laminar plumes and fires [6,29].

To provide a comparison to our numerical data, we can use the empirical relation of Cetegen and Ahmed [30] for the fundamental puffing frequency of a buoyant reacting jet. Their experiments showed that the dominant Strouhal number is given by

$$St = 0.8Ri^{0.38} \tag{16}$$

where $Ri = (1 - \rho_0/\rho_a) \cdot gD/U_0^2$ is the Richardson number. For our case, $\rho_0/\rho_a = 0.533$, $Ri = 0.29$ and this empirical formula predicts $St = 0.51$ which is very close to our numerical value of $St = 0.51$. This confirms that our LES gives reasonably accurate results under current grid resolution and numerical scheme. The pulsation frequency has been confirmed to be independent of the flame temperature or heat release rate [30] and Reynolds number [4]. Such an instability is purely induced by buoyancy via the baroclinic term which strongly depends on the Froude number and density ratio $\rho_0/\rho_a$ and is weakly dependent on the shear-layer thickness. With the same density ratio $\rho_0/\rho_a$ a similar result is expected in the presence and absence of the chemical reaction. *The puffing frequency appears to be independent of the reacting/nonreacting nature of the plume* [24].

Also shown in Fig. 6 are the power spectra of POD-reconstructed fluctuating radial velocities at the transitional downstream location $x/D = 9$; this location marks the effective end of the potential core. Reconstruction using 12 modes is in good agreement with the instantaneous data obtained from LES. Interestingly, the reconstruction

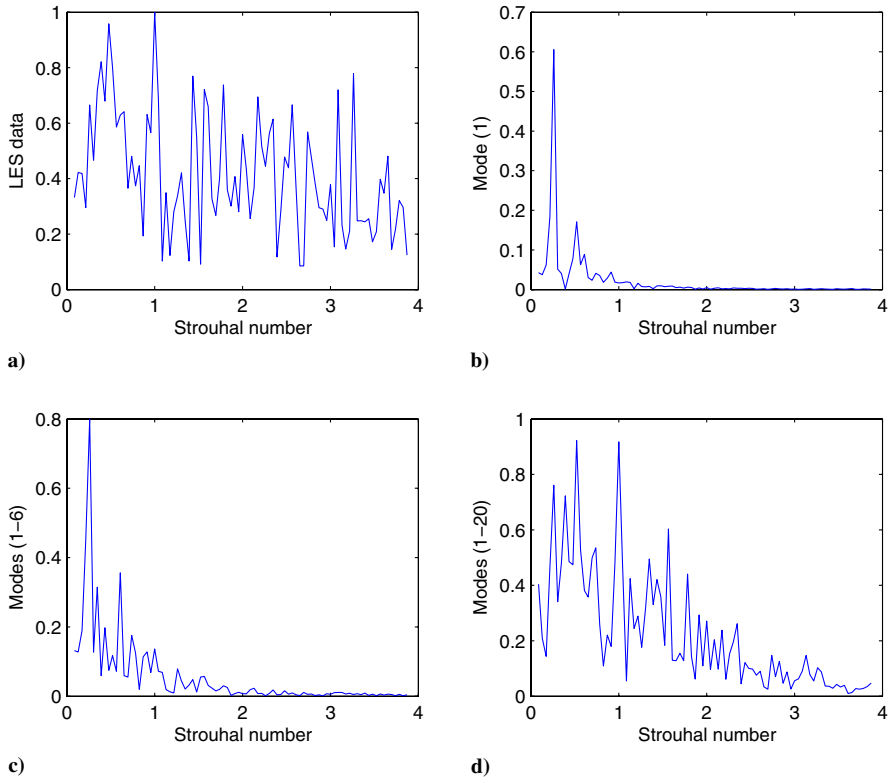


**Fig. 7 Normalized Fourier amplitudes of the fluctuating centerline radial velocities in the turbulent region $x/D = 11$. Shown are results obtained from a) the LES data; and POD reconstructions using b) one mode; c) the first 6 modes (note the predominance of the subharmonic); and d) 20 modes similar to LES data.**

shows a dominating subharmonic frequency rather than fundamental frequency as shown in the LES data. This points to the formation of a large-scale structure, which could be related to vortex merging downstream.

Finally, we examine the FFT amplitudes in the turbulent region at $x/D = 11$ (Fig. 7). Shown in this figure are results for the LES data, and POD reconstructions using the 1, 6, and 20 modes. The Fourier analysis from the reconstructions using 1 or 6 modes reveals dominant peaks at the subharmonic frequencies found in the near-field and transitional regions. This further illustrates a vortex merging behavior in the buoyant reacting jet. The Fourier amplitudes using 20 modes closely resembles the LES data. Although only the radial velocities were employed in the POD analysis, these results suggest the possibility of an inverse cascade of energy. In conclusion, *the laminar vortex structures characterizing the near field do persist and merge into even larger scales in the turbulent region, although they become masked amidst the turbulent spectrum.* POD analysis thus provides a powerful tool by which such information can be extracted, with the low-order eigenfunctions functioning effectively as low-pass filters.

## IV. Conclusions

In this work a transient buoyant jet diffusion flame of a moderate Reynolds number ($Re = 1000$) and has been simulated by LES. Repeatable and self-sustained shedding of toroidal vortical structures is observed in the laminar near-field region. Further downstream, the flow undergoes a transition to turbulence and the large vortical structures break down into small-scale eddies. We have employed the POD method to analyze the two-point correlation variances of the fluctuating temperatures and velocities generated from LES. The POD analyses are performed on 2-D plane sections of the flowfield taken along the streamwise and transverse directions. Within the laminar near field, it was found that only the first few eigenfunctions are necessary to capture the large-scale coherent structures. Additional eigenfunctions are required to characterize the flow details of the energetic structures in the transitional and turbulent regions. For example, in the near field less than 10 eigenmodes contain 90% of the energy; in contrast, approximately 36 eigenmodes are required in the transitional and turbulent regions.

The POD method has also been used to analyze the temporal fluctuations of the flow. In the near field the dominant vortex-shedding frequency obtained from Fourier analysis agrees well with experimental data of Cetegen [4]. A single POD mode is found to be sufficient to identify the fundamental shedding frequency and its first harmonic. In the transitional and turbulent regions, the low-order eigenmodes reveal the dominance of subharmonic frequencies indicating of vortex merging downstream. The POD technique enables the detection of these frequencies within the turbulent spectrum that otherwise would not be evident from Fourier analysis of the raw LES data. This is further indication of the power of this analytical tool.

Perhaps the most interesting and significant outcome of this work is the clear evidence of the persistence of the initial jet structure in the downstream flow as the jet transitions into turbulence. This finding is not at all obvious from the LES simulation data and is only revealed through the calculation of the POD modes. The validity of this finding, obtained from a 2-D POD analysis in this present work, is unlikely to be impacted by a fully 3-D POD analysis of the flowfield.

## Acknowledgments

This work was supported by the U.S. Air Force Office of Sponsored Research under the grant USAF 49620-02-1-0230. The authors would like to thank R. D. Prabhu for his helpful comments offered in the preparation of this article.

## References

[1] Ricou, F. P., and Spalding, D. B., "Measurements of Entrainment by Axisymmetrical Turbulent Jets," *Journal of Fluid Mechanics*, Vol. 11, 2006, pp. 21–32. doi:10.1017/S0022112061000834

[2] Papanicolaou, P. N., and List, E. J., "Investigations of Round Vertical Turbulent Buoyant Jets," *Journal of Fluid Mechanics*, Vol. 195, 2006, pp. 341–391. doi:10.1017/S0022112088002447

[3] Hamins, A., Yang, J. C., and Kashiwagi, T., "An Experimental Investigation of the Pulsation Frequency of Flames," *Proceedings of the Combustion Institute*, Vol. 24, No. 1, 1992, pp. 1695–1702. doi:10.1016/S0082-0784(06)80198-0

[4] Cetegen, B. M., *Physics of Fluids*, Vol. 9, No. 12, 1997, pp. 3742–3753. doi:10.1063/1.869512

[5] Yuan, T., Durox, D., and Villermaux, E., "An Analogue Study for Flame Flickering," *Experiments in Fluids*, Vol. 17, No. 5, 1994, pp. 337–349. doi:10.1007/BF01874414

[6] Mell, W. E., Mcgrattan, K. B., and Baum, H. R., "Numerical Simulation of Combustion in Fire Plumes," *Proceedings of the Combustion Institute*, Vol. 26, No. 1, 1996, pp. 1523–1530. doi:10.1016/S0082-0784(96)80374-2

[7] Lingens, A., Reeker, M., and Schriber, M., "Instability of Buoyant Diffusion Flames," *Experiments in Fluids*, Vol. 20, 1996, pp. 241–248. doi:10.1007/BF00192668

[8] Maxworthy, M., "The Flickering Candle: Transition to a Global Oscillation in a Thermal Plume," *Journal of Fluid Mechanics*, Vol. 390, 1999, pp. 297–323. doi:10.1017/S002211209900508X

[9] Buckmaster, J., and Peters, N., "The Infinite Candle and its Stability: A Paradigm for Flickering Diffusion Flame," *Proceedings of the Combustion Institute*, Vol. 28, 1986, pp. 1829–1836.

[10] Zhou, X., Luo, K. H., and Williams, J. J. R., "Vortex Dynamics in Spatio-Temporal Development of Reacting Plumes," *Combustion and Flame*, Vol. 129, Nos. 1–2, 2002, pp. 11–29. doi:10.1016/S0010-2180(01)00368-6

[11] Barlow, R. S., Smith, N. S. A., Chen, J.-Y., and Bilger, R. W., *Combustion and Flame*, Vol. 117, Nos. 1–2, 1999, pp. 4–31. doi:10.1016/S0010-2180(98)00071-6

[12] Klimenko, A. Y., and Bilger, R. W., *Progress in Energy and Combustion Science*, Vol. 25, No. 6, 1999, pp. 595–687. doi:10.1016/S0360-1285(99)00006-4

[13] Peters, N., *Twenty-First Symposium (International) on Combustion*, The Combustion Inst., Pittsburgh, PA, 1986, pp. 1231–1250.

[14] Jiang, X., and Luo, K. H., "Spatial Direct Numerical Simulation of the Large Vortical Structures in Forced Plumes," *Flow, Turbulence and Combustion*, Vol. 64, No. 1, 2000, pp. 43–69. doi:10.1023/A:1009950127478

[15] Jiang, X., and Luo, K. H., "Dynamics and Structure of Transitional Buoyant Jet Diffusion Flames with Side-Wall Effects," *Combustion and Flame*, Vol. 133, Nos. 1–2, 2003, pp. 29–45. doi:10.1016/S0010-2180(02)00539-4

[16] Grinstein, F. F., and DeVore, C. R., "Dynamics of Coherent Structures and Transition to Turbulence in Free Square Jets," *Physics of Fluids*, Vol. 8, No. 5, 1996, pp. 1237–1251. doi:10.1063/1.868895

[17] Zhou, X., Luo, K. H., and Williams, J. J. R., "Large-Eddy Simulation of a Turbulent Forced Plume," *European Journal of Mechanics B: Fluids*, Vol. 20, No. 2, 2001, pp. 233–254. doi:10.1016/S0997-7546(00)01117-1

[18] Berkooz, G., Holmes, P., and Lumley, J. L., "The Proper Orthogonal Decomposition in the Analysis of Turbulent Flows," *Annual Review of Fluid Mechanics*, Vol. 25, 1993, pp. 539–575. doi:10.1146/annurev.fl.25.010193.002543

[19] Citriniti, J. H., and George, W. K., "Reconstruction of the Global Velocity Field in the Axisymmetric Mixing Layer Utilizing the Proper Orthogonal Decomposition," *Journal of Fluid Mechanics*, Vol. 418, 2000, pp. 137–166. doi:10.1017/S0022112000001087

[20] Caraballo, E., Samimy, M., Narayanan, S., DeBonis, J., and Scott, J., "Application of Proper Orthogonal Decomposition to a High Speed Axisymmetric Jet," AIAA Paper 2001-2783.

[21] Manhart, M., "Vortex Shedding from a Hemisphere in a Turbulent Boundary Layer," *Theoretical and Computational Fluid Dynamics*, Vol. 12, No. 1, 1998, pp. 1–28. doi:10.1007/s001620050096

[22] Prabhu, R. D., Collis, S. S., and Chang, Y., "The Influence of Control on Proper Orthogonal Decomposition of Wall-Bounded Turbulent Flows," *Physics of Fluids*, Vol. 13, No. 2, 2001, pp. 520–537. doi:10.1063/1.1333038

[23] Gordeyev, S. V., and Thomas, F. O., "Coherent Structure in the Turbulent Planar Jet. Part 2. Structural Topoloy via Pod Eigenmoce Projection," *Journal of Fluid Mechanics*, Vol. 460, 2002, pp. 349–380. doi:10.1017/S0022112002008364

[24] Zhou, X., and Hitt, D. L., "Pod Analysis of Coherent Structures in a Transient Buoyant Jet," *Journal of Turbulence*, Vol. 5, No. 1, 2004, pp. 28–28(1). doi:10.1088/1468-5248/5/1/028
[25] Glauser, M. N., and George, W. K., "An Orthogonal Decomposition of the Axisymmetric Jet Mixing Layer Utilizing Cross-Wire Velocity Measurements," *Proceedings of the Sixth Symposium on Turbulent Shear Flows*, ONERA, Toulouse, France, 1987, pp. 101.1–101.6.
[26] Sirovich. L., "Turbulence and the Dynamics of Coherent Structures," *Quarterly of Applied Mathematics*, Vol. XLV, No. 3, 1987, pp. 561–590.
[27] Ma, X., and Karniadakis, G. E., "A Low-Dimensional Model for Simulating Three-Dimensional Cylinder Flow," *Journal of Fluid Mechanics*, Vol. 458, 2002, pp. 181–190. doi:10.1017/S0022112002007991
[28] Jiang, X., and Luo, K. H., *Flow, Turbulence, and Combustion*, Vol. 64, No. 1, 2000, pp. 43–69. doi:10.1023/A:1009950127478
[29] Ghoniem, A. F., Lakkis, I., and Soteriou, M., "Numerical Simulation of the Dynamics of Large Fire Plumes and the Phenomenon of Puffing," *Proceedings of the Combustion Inst.*, Vol. 28, The Combustion Inst., Pittsburgh, PA, 1996, pp. 1531–1539.
[30] Cetegen, B. M., and Ahmed, T. A., *Combustion and Flame*, Vol. 93, Nos. 1–2, 1993, pp. 157–184. doi:10.1016/0010-2180(93)90090-P

M. Glauser
*Associate Editor*